

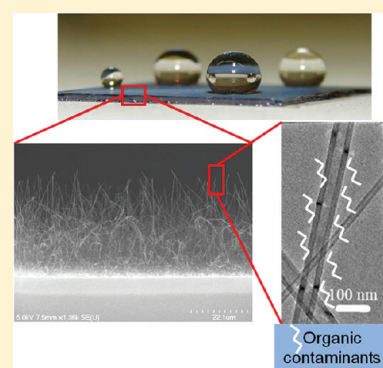
# Origins of Thermodynamically Stable Superhydrophobicity of Boron Nitride Nanotubes Coatings

Ludmila B. Boinovich,<sup>\*,†</sup> Alexandre M. Emelyanenko,<sup>†</sup> Andrei S. Pashinin,<sup>†</sup> Chee Huei Lee,<sup>‡</sup> Jaroslaw Drelich,<sup>§</sup> and Yoke Khin Yap<sup>\*,‡</sup>

<sup>†</sup>A.N. Frumkin Institute of Physical Chemistry and Electrochemistry, Russian Academy of Sciences, Leninsky prospect 31, 119991 Moscow, Russia

<sup>‡</sup>Department of Physics, and <sup>§</sup>Department of Materials Science and Engineering, Michigan Technological University, 1400 Townsend Drive, Houghton, Michigan 49931, United States

**ABSTRACT:** Superhydrophobic surfaces are attractive as self-cleaning protective coatings in harsh environments with extreme temperatures and pH levels. Hexagonal phase boron nitride (h-BN) films are promising protective coatings due to their extraordinary chemical and thermal stability. However, their high surface energy makes them hydrophilic and thus not applicable as water repelling coatings. Our recent discovery on the superhydrophobicity of boron nitride nanotubes (BNNTs) is thus contradicting with the fact that BN materials would not be hydrophobic. To resolve this contradiction, we have investigated BNNT coatings by time-dependent contact angle measurement, thermogravimetry, IR spectroscopy, and electron microscopy. We found that the wettability of BNNTs is determined by the packing density, orientation, length of nanotubes, and the environmental condition. The origins of superhydrophobicity of these BNNT coatings are identified as (1) surface morphology and (2) hydrocarbon adsorbates on BNNTs. Hydrocarbon molecules adsorb spontaneously on the curved surfaces of nanotubes more intensively than on flat surfaces of BN films. This means the surface energy of BNNTs was enhanced by their large curvatures and thus increased the affinity of BNNTs to adsorb airborne molecules, which in turn would reduce the surface energy of BNNTs and make them hydrophobic. Our study revealed that both high-temperature and UV-ozone treatments can remove these adsorbates and lead to restitution of hydrophilic BN surface. However, nanotubes have a unique capability in building a hydrophobic layer of adsorbates after a few hours of exposure to ambient air.



## INTRODUCTION

Nature has created many examples of highly water repellent (superhydrophobic) biological surfaces. Leaves of the lotus plant (*Nelumbo nucifera*) as well as nearly 200 other plant species are superhydrophobic due to micro- and nanosized asperities or hairs, which are coated with hydrophobic wax.<sup>1,2</sup> Wings of many insects,<sup>3–5</sup> feathers of birds,<sup>6,7</sup> and body parts of semiaquatic and aquatic insects<sup>8–12</sup> are also superhydrophobic due to a combination of organic coatings and fine biological structures. As inspired by nature, researchers could fabricate superhydrophobic surfaces by organic coatings and microscopic surfaces.<sup>13,14</sup> The prospect of self-cleaning windows, counter tops, fabrics, and even microrobots that can walk on water drives the innovations into designing more sophisticated and durable superhydrophobic coatings.

The uses of polymeric and organic superhydrophobic surfaces are limited by their short lifetime, due to mechanical erosion and heat degradation. Many strong acids, bases, and UV irradiation from the sunlight accelerate instability and degradation of these coatings. The search for superhydrophobic inorganic materials is thus important for applications in sporadic harsh environment. Nature cannot be mimicked here as there is no known natural inorganic example displaying

superhydrophobicity. The design of ceramic coatings with superhydrophobicity is complicated by the hydrophilic properties of these materials, commonly known as high surface energy materials.

The possibility of achieving the thermodynamically stable superhydrophobic and highly hydrophobic state on the rough surface of hydrophilic materials has been widely discussed in the literature.<sup>15–20</sup> The main points raising heated debates are: (1) whether such state can be considered as thermodynamically stable or it is simply a metastable one; and (2) what physical mechanisms, if any, can provide the manifestation of hydrophobicity for high-energy materials. These points arise from comparison between the experimental findings and the theoretical predictions. We will elucidate below the contradiction that follows from such comparison.

The main peculiarity of liquid spreading on a rough surface is the existence of two different wetting regimes: homogeneous and heterogeneous ones (Figure 1). Both regimes correspond to minima in the Gibbs free energy of the three-phase system containing a wetted substrate, wetting liquid, and surrounding

Received: August 9, 2011

Published: December 7, 2011

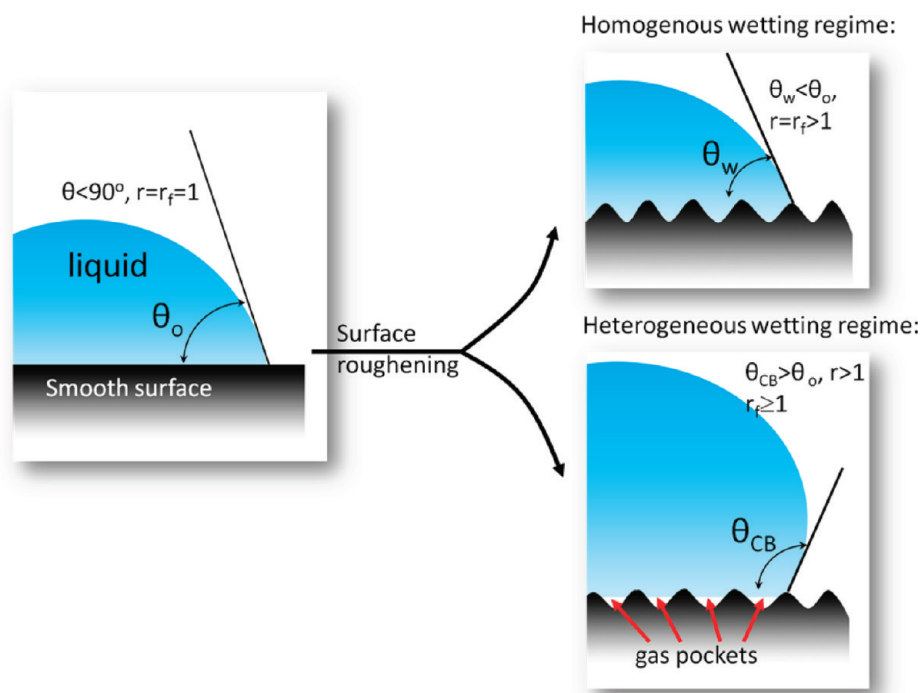


**Figure 1.** Schematic drawings of wetting regimes for a liquid droplet on a rough solid surface.

phase (vapor or other liquid).<sup>21</sup> Wettability in homogeneous regime can be indicated by the water contact angle ( $\theta_w$ ) as described by the Wenzel equation<sup>22</sup> (also often referred to as the Wenzel–Derjaguin equation in the Russian literature<sup>23</sup>):

$$\cos \theta_w = r \cos \theta_0 \quad (1)$$

and is determined by the chemical composition of surface layer represented in the above equation through the Young contact angle  $\theta_0$  and by the roughness parameter  $r$ . Thus, the roughness of surface enhances its hydrophobicity if  $\theta_0 > 90^\circ$  and improves wettability for  $\theta_0 < 90^\circ$ .

In the heterogeneous regime, the contact angle can be described using the Cassie–Baxter equation:<sup>21,24</sup>

$$\cos \theta_{CB} = r_f f \cos \theta_0 - 1 + f \quad (2)$$

and the main factors affecting the contact angle value are the chemical composition of the surface layer, associated with  $\theta_0$ , the roughness of wetted area  $r_b$  and the portion of substrate surface wetted by testing liquid,  $f$ .

As follows from the analysis of the Cassie–Baxter eq 2, in the heterogeneous wetting regime, one can manipulate  $\theta_{CB}$  on the rough surface by simply varying the surface topography and, as a result, the portion of wetted solid area  $f$ . Theoretically, therefore, a superhydrophobicity, with water contact angle higher than  $150^\circ$ , can be achieved on any intrinsically hydrophilic material with  $0^\circ < \theta_0 < 90^\circ$ . For example, material with  $\theta_0 = 55^\circ$  would need to be roughened to produce nail-shaped protrusions with flat heads such that water meniscus may pin at the heads edges and less than 9% of the solid surface is wetted by water. Such rough surfaces are difficult to fabricate, although it is less challenging when roughness is introduced by the growth of nanomaterials. Even when accomplished by such approaches, a superhydrophobic state for the hydrophilic material ( $\theta_0 < 90^\circ$ ) is only the realization of metastability. As it was shown by thermodynamic analysis,<sup>21,25–27</sup> the smallest of the two possible contact angles, associated with homogeneous

and heterogeneous wetting regimes, corresponds to the lower Gibbs free energy, and therefore to the higher thermodynamic stability. For hydrophilic materials (with  $\theta_0 < 90^\circ$ ), effective contact angles in the homogeneous regime will always be less than in the heterogeneous regime, and, according to the thermodynamics, the hydrophilic state of such materials with rough surface is expected to be more thermodynamically favorable than the hydrophobic one.

When the substrate surface possesses a complex topography, the Gibbs free energy of the three-phase system can have several local minima, separated by energy barriers.<sup>28–30</sup> Such systems can exist in metastable states with the spontaneous transition to more stable states at low barriers. If the potential barrier is high enough, which is typical for the multilevel (re-entrant) surface topography, the metastable heterogeneous wetting regime can be frozen for some time and reveals itself as the robust one.<sup>31,32</sup> For such surfaces, the transition from the metastable heterogeneous to the stable homogeneous wetting regime can be provoked through a supply of external energy (i.e., vibration, pressing the droplet against the substrate, hydrostatic pressure at deep immersion, or due to the kinetic energy of the falling droplet<sup>27,33–36</sup>). Metastable superhydrophobicity can hardly be used in practical applications due to the transition to higher stability of the homogeneous wetting regime with the effective contact angle  $\theta_w < 90^\circ$ .

At the same time, a few studies appeared in the literature (see, for example, refs 36–38), where the formation of stable superhydrophobic states on the surface of ceramic materials having high surface energy (and thus with  $\theta_0 < 90^\circ$ ) was reported. Unfortunately, the stability of the superhydrophobic state and the forming mechanisms of such state were not discussed in refs 36–38.

Here, we analyze both homogeneous and heterogeneous wetting regimes for boron nitride nanotube (BNNT) coatings in details. The bulk boron nitride, as follows from theoretical calculations, is the material having high-energy surfaces.<sup>39,40</sup> We

demonstrate that the superhydrophobic state of the BNNT coating can be thermodynamically stable, which results from a spontaneous adsorption of hydrocarbons onto the highly curved surfaces of BNNTs. A remarkable property of BNNT coating is the self-restoration of hydrocarbon layer adsorbed in a few hours after high temperature adsorbate removal.

## MATERIALS AND METHODS

In this Article, we have studied coatings made of short and long BNNTs grown on silicon substrate as described in refs 37,38,41 and hexagonal phase boron nitride (h-BN) thin films deposited by a pulse laser deposition (PLD) technique.<sup>37</sup> The subdividing of BNNTs into two groups<sup>37</sup> is determined by the temperature and time of synthesis and the average length of nanotubes. If not mentioned otherwise, the testing was performed on as-grown samples without additional cleaning. The cases when different cleaning procedures were used will be discussed separately. Two major cleanings reported in this Article were done with solvent and under UV light. We washed selected samples with a C<sub>2</sub>H<sub>5</sub>OH–H<sub>2</sub>O (1:1) mixture at 80° for 2 h. During washing, the mixture was replaced eight times, and after such procedure the samples were rinsed in cold deionized water and dried during 2 days. Selected samples were inserted into a UV cleaner (Bioforce Laboratories) and exposed to UV irradiation for 90–120 min.

Fourier transformed infrared (FTIR) spectroscopy at a grazing angle of 80° (Perkin-Elmer 2000 Fourier spectrometer equipped with Spectra-Tech FT-80 Grazing Angle Accessory), 800 scans and 4 cm<sup>-1</sup> resolution, was used to analyze the chemical makeup and contamination of BNNT coatings and its variation after heat treatments. Also, attenuated total reflectance FTIR spectroscopy using ZnSe crystal, at operating conditions of 1000 scans and 4 cm<sup>-1</sup> resolution was used in the examination of organic contaminants on selected BNNTs films before and after cleaning in the UV cleaner.

The substrate temperature was controlled by the Peltier thermo-electric module (TV127-1,4-1,15–80 W).

Scanning electron microscopy (SEM) images were obtained with S-4700 field emission scanning electron microscope (SEM) (Hitachi) using 5 kV accelerating voltage and JSM U3 SEM (JEOL) using 25 kV accelerating voltage. The JSM instrument was equipped with a WinEDS attachment for energy dispersive analysis of X-rays and a DISS digital scanning system (Getac).

The study of the degree of hydrophobicity for the deposited coatings and its degradation was based on contact angle measurements. We used the method of digital video image processing of sessile droplets. The homemade experimental setup for recording optical images of sessile droplets and software for subsequent determination of droplet parameters using Laplace curve fitting routine were described earlier.<sup>42,43</sup> A monochrome digital camera Pixelink PL-B686MU with space resolution 1280 × 1024, color resolution 256 gray levels, and time resolution 25 frames per second was used to capture the droplet images. To analyze the deterioration of hydrophobic state, deionized water was used as a testing liquid. Such choice of the liquid allows studying the evolution of contact angle and the process of interaction of substrate with water in situ. Typical time, necessary for equilibrating the initial shape of deposited droplet, did not exceed milliseconds, and in the following we will refer to the angle obtained in 2 s after the droplet deposition, as an initial contact angle. The measured initial contact angles, as follows from the behavior of contact diameter, correspond to advancing contact angles. Subsequent evolution of droplet shape is determined by many factors such as pinning of contact line in droplet spreading over rough surfaces, growth of precursor adsorption or wetting film in the vicinity of droplet, transition from the metastable to the stable regime of wetting, interaction of liquid with substrate resulting in variation of wetting due to alteration of chemical composition of substrate, and partial detachment of segments of coating from the coating/liquid interface.

To characterize the wetting of different coatings, initial contact angles for the 10–15 μL droplets were measured on five different surface locations for each sample, with the average angle for 10

consecutive images of the droplet being defined for each place. The reproducibility of the contact angle determination defined as the root-mean-square (rms) deviation of angles for 10 consecutive images of the droplet was better than 0.1°.

The stability of superhydrophobicity was studied by the evolution of water contact angle, base diameter of water droplet, and liquid surface tension as a function of time. To conduct these measurements, a tested sample was placed inside the experimental chamber on the top of a fine positioner, which allows adjustment of the sample tilt with the accuracy of 0.05°. The humidity inside the experimental chamber was maintained at 100%, as described in ref 44. Although 100% humidity atmosphere has the vapor pressure undersaturated with respect to the convex droplet surface, the water droplet with 2 mm contact diameter can be stored in such a system more than 15 days without noticeable variation in droplet size, caused by evaporation. The low evaporation rate and simultaneous measurement of contact angle, droplet base diameter, and liquid/vapor surface tension made it possible to distinguish between the decrease in the contact angle caused by evaporation of the droplet and that related to the hydrophilization of the substrate as a result of its interaction with water.

To measure the rolling angle, the 10–15 μL droplets were deposited onto the surface. After the initial droplet shape equilibration, the manipulation with an angular positioner allowed one to change the sample surface tilt in a controllable manner and detect the rolling angle as a result of averaging over five different droplets on the same substrate.

## RESULTS AND DISCUSSION

The initial advancing angles, as well as rolling angles for all BNNT coatings studied in this Article, are presented in Table 1.

Table 1. Contact and Rolling Angles for Samples

| sample                        | contact angle, deg | rolling angle, deg |
|-------------------------------|--------------------|--------------------|
| silicon wafer without coating | 44.8 ± 1.7         |                    |
| h-BN film deposited by PLD    | 55.3 ± 1.5         |                    |
| short BNNT                    | 167.2 ± 3.8        | 6.1 ± 4.6          |
| long BNNT                     | 165.9 ± 2.3        | 10.7 ± 4.9         |

The contact angles, characteristic to the h-BN film and to the silicon substrate, are shown in Table 1 as well. As shown, both the Si substrate and the h-BN film are hydrophilic, while the as-grown BNNT coatings are superhydrophobic.

The h-BN film has smooth morphology with rms = 21.9 ± 1.7 nm and arithmetic R<sub>a</sub> = 14.8 ± 1.3 nm.<sup>37</sup> The advancing contact angle for the h-BN film is ~55°, which is substantially less than those for hydrophobic materials with water contact angle larger than 90°. For example, polyethylene with the surface energy of 31–36 mJ/m<sup>2</sup> demonstrates contact angle with water in the range of 90–100°.<sup>45,46</sup> The reported surface energy of BN (cubic phase, c-BN) materials range from ~40 mJ/m<sup>2</sup> for thin films<sup>47,48</sup> to >3000 mJ/m<sup>2</sup> for bulk samples.<sup>39,40</sup> Interestingly, surface energy as low as 27 mJ/m<sup>2</sup> was reported for BNNTs;<sup>49</sup> we will return to this issue later.

All of the reported contact angles and surface energies suggest on the hydrophilic state of macroscopic BN surfaces. In contrast, contact angles on BNNT coatings measured here (Table 1) are >150° and consistent with the reported data.<sup>37</sup> These are typical for superhydrophobic materials. The superhydrophobic nature of BNNT coatings was also confirmed by weak adhesion of water droplets to BNNT coatings as water droplets easily rolled off the coating (rolling angle <10–15°; Table 1). The typical images of water droplets on BNNT coatings are shown in Figure 2. As shown in the cross-section SEM view, our BNNTs are merely vertically

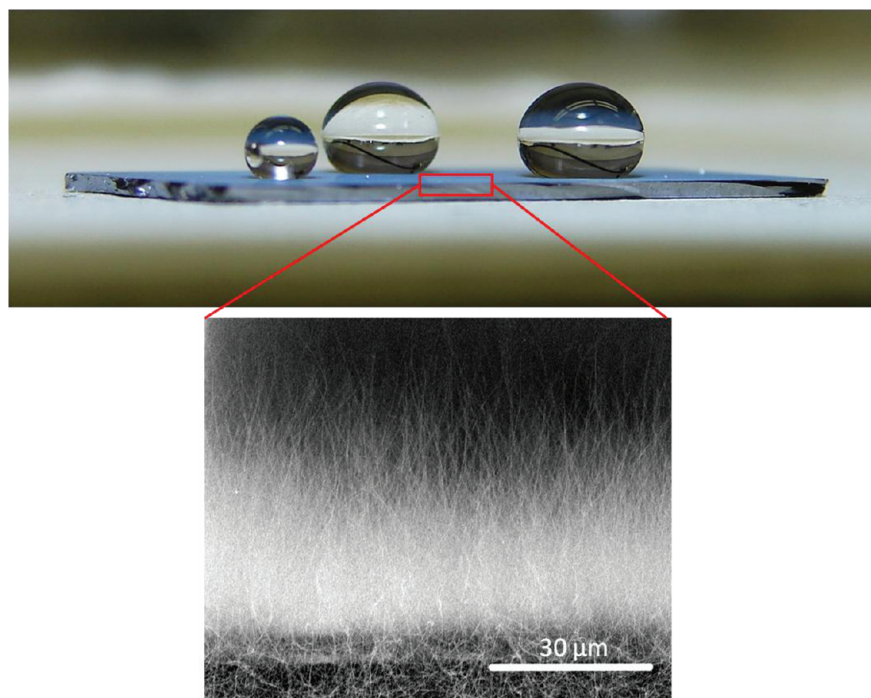


**Figure 2.** Images of water droplets on BNNTs coated on a Si substrate (top) and the cross-sectional view of the sample showing BNNTs grown vertically aligned on the substrate (bottom).

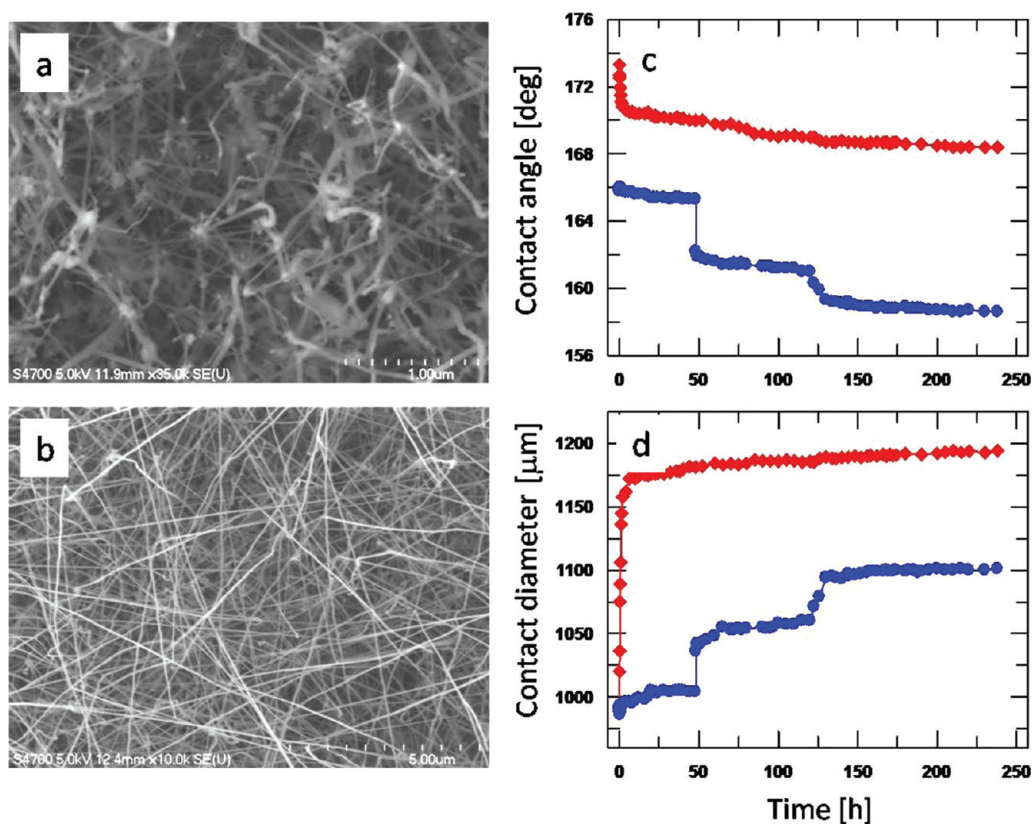


**Figure 3.** SEM images of samples with short (a) and long (b) BNNTs. Evolution of contact angle (c) and contact diameter (d) with time for the samples with short (◆) and long (●) BNNTs.

aligned on the substrate surface with the tips of BNNTs randomly pointing upward.

Thus, the nature of superhydrophobic state of BNNT coatings has to be discussed. Three hypotheses were tested

here: (1) the stability of superhydrophobicity of BNNT coatings, (2) the effect of curvature on the wettability of individual nanotubes, causing an increase in the Young contact angle to  $\theta_0 > 90^\circ$ , and (3) the adsorption of organic

contaminants onto the BNNT surface giving sufficiently low surface energy and  $\theta_0 > 90^\circ$ .

**Stability of Superhydrophobic State.** The stability of superhydrophobicity was analyzed by monitoring the evolution of contact angle and the base diameter of water droplet and liquid surface tension of the droplet. For samples coated with short (Figure 3a) and long (Figure 3b) BNNTs, the contact angles decreased only by a few degrees after 10 days as shown in Figure 3c. The superhydrophobic state was maintained with final contact angles of  $\sim 158^\circ$  and  $\sim 168^\circ$  for long and short BNNTs, respectively. Also, despite such a long exposure time, each BNNT coating preserved low wetting hysteresis, and water droplets continued to rolled off the samples at low sample tilts,  $<10\text{--}15^\circ$ .

A decrease in contact angle was also accompanied by an expansion of the droplet base diameter (Figure 3d). This phenomenon is, most likely, due to the formation of water adsorption film on nanotubes.<sup>50</sup> As shown in Figure 4, smaller

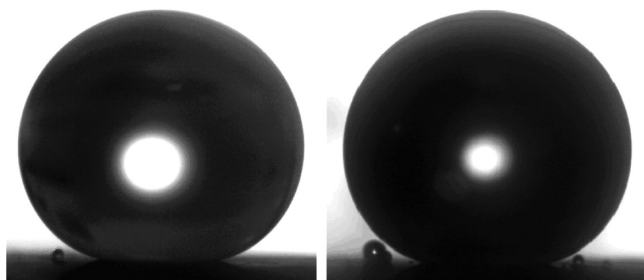


**Figure 4.** Images of the sessile water droplet on the surface of samples coated with short BNNTs surrounded by small droplets that nucleated and grew during long-time tests.

water droplets nucleated and grew near the base of (macroscopic) sessile droplet after several hours during the stability tests. The growth of microdroplets was particularly noticeable for short BNNTs and unambiguously indicates the presence of water-soluble constituent on the coating. The analysis of IR absorbance spectra of short BNNTs (Appendix) allowed us to associate water-soluble substances with  $B_xO_y$  groups. Traces of these oxides on BNNTs could lead to the nucleation of aqueous microdroplets with the equilibrium vapor pressure smaller than the saturated value above bulk water. Thus, in the experimental chamber, supersaturation with respect to aqueous solution holds, which promotes growth of microdroplets. The growth of the microdroplet volume is obvious as one compares the sizes of the microdroplets to that of the larger sessile droplet that we introduced (Figure 4).

We have also tested the stability of superhydrophobicity by vibrating the BNNT coatings with deposited water droplets. It was suggested<sup>51</sup> that stable (equilibrium) contact angles can be measured for both heterogeneous and rough surfaces after applying external mechanical energy to a solid in contact with a wetting liquid. Our experiments showed that vibrations could distort the shape of water droplets on BNNT films, but their contact angles restored in a few minutes after termination of the vibrations.

For further understanding of the mechanism of the stable superhydrophobicity of our samples, we have forced the transition of wetting regime on BNNT coatings from heterogeneous to homogeneous. This was accomplished through local substrate cooling. We used a Pelitier device to decrease the temperature of the sample to  $T = 1^\circ\text{C}$  while keeping the temperature of the surrounding vapor phase at  $T = 20^\circ\text{C}$ . Such a temperature gradient initiated the condensation of water vapor on BNNTs due to the difference in chemical potential of water molecules at different temperatures. Next, we

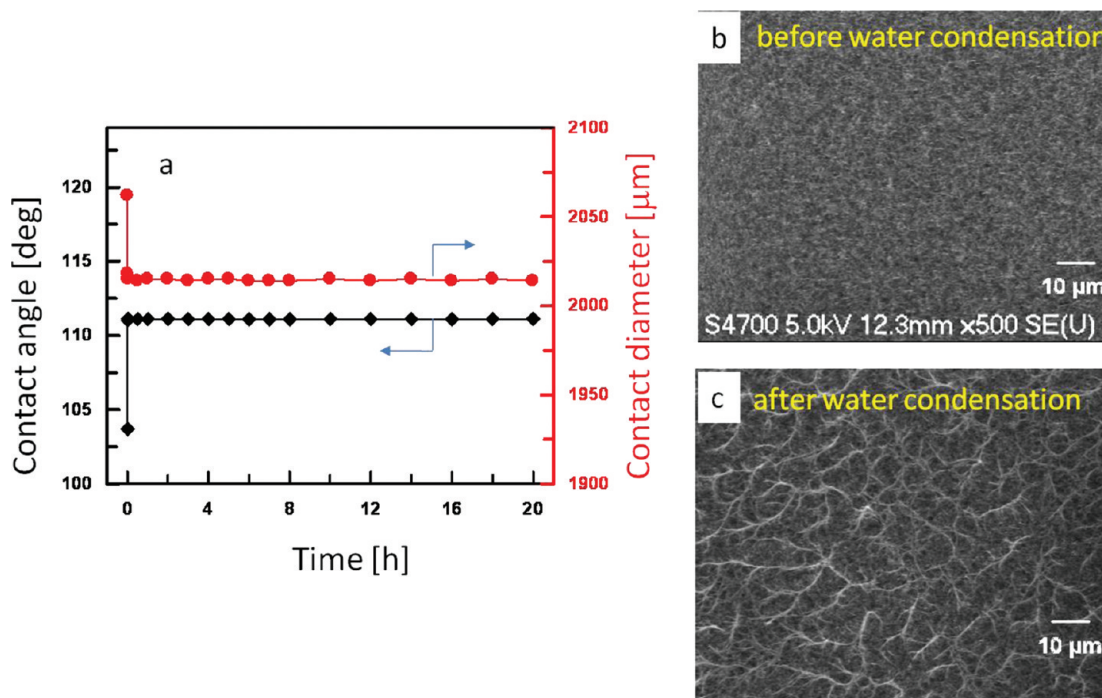


**Figure 5.** The time evolution of the contact angle (◆) and the contact diameter (●) on long BNNTs during the warming process from 1 to 20 °C (a). SEM images (top view) of the sample before (b) and after (c) the water condensation experiment. Bundling of BNNTs is clearly seen after the experiment.

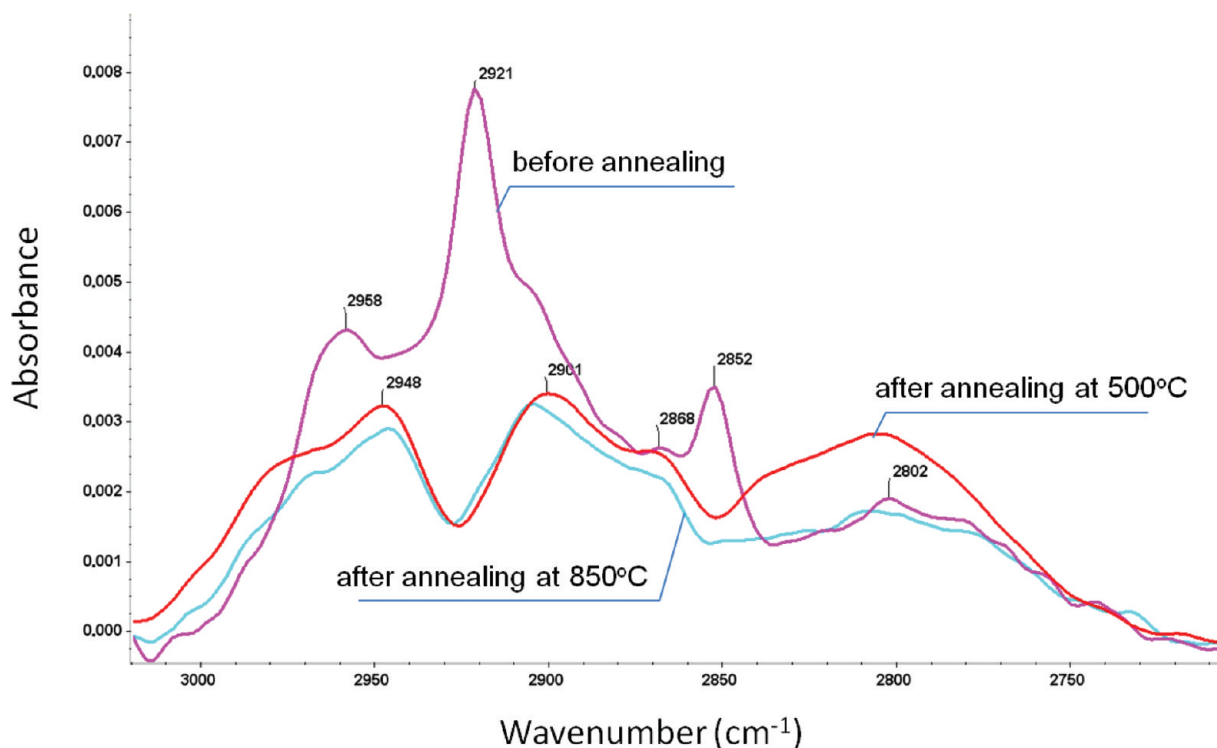


**Figure 6.** IR absorbance spectra of long BNNTs before and after heat treatment at 500 and 850 °C. The presented range of spectra contains bands associated with CH stretching vibrations in  $\text{CH}_{(n)}$  groups of various organic compounds.<sup>55</sup>

placed a sessile droplet on top of a cooled sample (coating with long BNNTs). As shown in Figure 5a, the water droplet acquired homogeneous wetting regime, with an initial contact angle of  $\theta = 103^\circ$ . The contact angle increased quickly to  $111^\circ$  and then remained stable for 20 h after we allowed the sample to return to room temperature by turning off the Peltier device. This was accompanied by a quick decrease in the droplet base diameter, which was then stable for 20 h.

Two main conclusions can be deduced from the data presented in Figure 5a. First, according to eq 1, to satisfy the Wenzel wetting regime for  $\theta_W > 103^\circ$ , the Young contact angle has to be  $\theta_0 > 90^\circ$ . Second, although the evident increase in the contact angle and decrease of the contact diameter took place, the superhydrophobic state of our sample was not fully restored even when equilibration condition was established at room temperature. Such behavior of the drop might be related to either inverse transition from homogeneous to heterogeneous wetting regime or variation of surface energies of three contacting interfaces due to a raise in the substrate temperature, decrease in vapor oversaturation and evaporation of water from intertube space that condensed earlier. As shown in Figure 5b and c, irreversible bundling and flattening of nanotubes took place after water vapor condensation on the sample. This is most likely responsible for the lack of full restoration of superhydrophobic state as the  $f$  value (eq 2) became much larger for the flattened sample.<sup>37</sup> The phenomenon described above was detected in the experiments with both short and long nanotubes.

**Influence of BNNT Curvature on the Wettability of Individual Nanotube.** In the previous section, we have shown that the superhydrophobic state of BNNT coatings is thermodynamically stable, and therefore the Young contact angle on BNNTs must be larger than  $90^\circ$ . Because the contact angle on our h-BN film is about  $55^\circ$  (Table 1), we believe that

the higher contact angles detected on BNNTs are related to their large surface curvature. The comparison of contact angle data for flat film, measured in this study, and that for individual boron nitride nanotubes with the diameter 40 nm studied with the Wilhelmy method in ambient conditions<sup>49</sup> supports this hypothesis. In fact, it is known that contact angles depend on the curvature of the contact surfaces.<sup>36,52</sup> The increase in curvature of convex surfaces was shown to increase the water contact angle as the radius of contact surface becomes comparable to the range of action of surface forces. This effect is especially important for systems with very strong and long ranged surface forces and may cause even transition from hydrophilic state with  $\theta_0 < 90^\circ$  to hydrophobic state with  $\theta_0 > 90^\circ$ . However, the curving of h-BN sheets is not the only reason for the increased contact angle value, as will be discussed below.

**Hydrophobization of BNNTs Due to the Spontaneous Adsorption of Organics.** Another reason for the hydrophobic state of our BNNT coatings is related to the adsorption of organic molecules. As discussed earlier, although the surface energy for h-BN is unknown to us, theoretical calculations give very high values for bulk c-BN.<sup>39,40</sup> Chemical and physical adsorption activity on the surface of various high energy materials is often driven by the tendency to reduce the total free (Gibbs) energy of the system by diminishing the surface energy part. Thus, from the view of thermodynamics, the surfaces of BNNTs could have been enhanced by adsorbates that decrease their surface energy. To confirm the adsorption of organic contaminants from the environment on BNNTs, infrared (IR) absorption spectra were measured at a grazing angle of  $80^\circ$ . This was carried out for coatings with both short and long BNNTs.

As shown in Figure 6, the characteristic alkyl C–H bond stretching vibrations of  $\text{CH}_2$  and  $\text{CH}_3$  groups were ubiquitous

detected from our samples in the range 3000–2700  $\text{cm}^{-1}$ . This is direct evidence of the presence of hydrocarbon contaminants on the surface of our BNNTs. We will discuss the IR spectra after annealing at 500 and 850  $^{\circ}\text{C}$  hereafter.

To elucidate the nature of such adsorption, physical versus chemical, two types of experiments were performed. First, we attempted to remove physically adsorbed contaminations by washing the samples in 1:1  $\text{C}_2\text{H}_5\text{OH}-\text{H}_2\text{O}$  mixture at 80 $^{\circ}$  for 2 h. During washing, the mixture was replaced eight times. After washing, the samples were rinsed with cold deionized water and dried slowly for 2 days. The initial contact angles measured for the washed samples are presented in Table 2. As compared to

**Table 2. Initial Contact Angles for Samples Washed with a 1:1  $\text{C}_2\text{H}_5\text{OH}-\text{H}_2\text{O}$  Mixture**

| sample                     | contact angle, deg |
|----------------------------|--------------------|
| h-BN film deposited by PLD | 49.2 $\pm$ 2.4     |
| short BN NT                | 143.5 $\pm$ 1.8    |
| long BN NT                 | 135.3 $\pm$ 2.3    |

those measured from as-grown samples (Table 1), obvious decreases in contact angles were detected for all washed samples, including BNNT coatings and h-BN film. The observed drop in contact angle could be the result of either incomplete removal of physically adsorbed organic contaminants from the surfaces or readsorption of contaminants during drying. However, washing and drying the BNNT coatings can cause bundling as a result of capillary forces for liquid meniscus acting between BNNTs,<sup>37</sup> and the initial contact angles were rarely restored for washed samples.

To avoid bundling of BNNTs, we attempted to remove the organic contaminants by extensively exposing the BNNT samples to UV-ozone etching in a UV cleaner designed for the cleaning of AFM cantilever tips from hydrocarbons.<sup>53</sup> We found that the contact angles on BNNT coatings sometimes decreased only 12–20 $^{\circ}$  after 90 min UV-ozone treatment but typically dropped to zero after 2 h of cleaning. Figure 7 shows

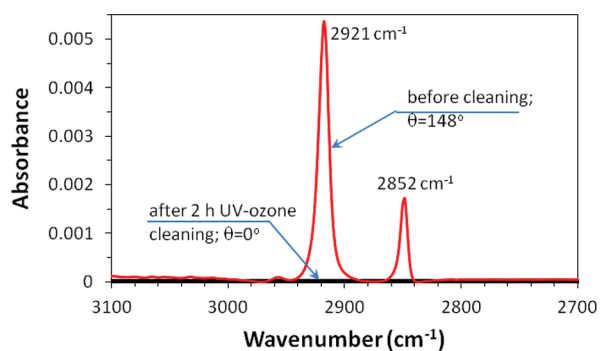


**Figure 7.** ATR-IR absorbance spectra of long BNNTs before and after cleaning in the UV cleaner for 2 h.  $\theta$  is the average advancing contact angle measured for a water droplet.

the CH asymmetric (2921  $\text{cm}^{-1}$ ) and CH symmetric (2852  $\text{cm}^{-1}$ ) bands of  $\text{CH}_2$  groups associated with organics contaminating surfaces of the BNNTs. After being cleaned in the UV cleaner for 2 h, the intensity of these bands drops practically to zero (to the level of noise), but slowly restores after sample exposure to the laboratory air (as will be discussed later in this section). The results of this experiment confirm the

presence of organics on BNNTs and BNNTs affinity toward airborne contaminants.

Finally, we attempted to remove both physically and chemically adsorbed organic contaminants by heat treatment. BNNTs were reported to be thermally stable at temperature above 1100  $^{\circ}\text{C}$ .<sup>54</sup> In our studies, the heat treatment at different temperatures was performed in a thermogravimetric chamber (TA Instruments). After being heated to a selected temperature, the samples were heat treated for an hour, and then cooled to room temperature, with constant flow of either pure argon or in air throughout the whole process. The initial contact angles, measured 10 min after the treatment in argon for samples coated with short ( $\bullet$ ) and long ( $\diamond$ ) BNNTs, are shown in Figure 8a. For comparison, the initial contact angles for samples coated with long BNNTs after heat treatment in air ( $\blacklozenge$ ) are also shown.

As shown in Figure 8a, similar results are detected for samples coated with long BNNTs after heat treatment in argon and air. This means insignificance of oxidation (if present) on our BNNTs. A similar trend is observed for samples coated with short BNNTs after heat treatment in argon ambient. A gradual deterioration of hydrophobic state (decrease in contact angles) was recorded for all of these samples after heat treatments at temperatures higher than  $\sim 400$   $^{\circ}\text{C}$ . The transition to hydrophilic state occurred at about 800  $^{\circ}\text{C}$  (contact angle  $< 90^{\circ}$ ), and contact angles dropped to  $\sim 20$ – $45^{\circ}$  after annealing at 850  $^{\circ}\text{C}$ . The decrease in contact angles is accompanied by the simultaneous increase in statistical variation of the contact angle. We attribute these behaviors to two independent phenomena: (1) the removal of organic adsorbates and (2) the gradual distortion of the BNNT networks.

As shown in Figure 2, our as-grown BNNTs are partially vertically aligned with their tips pointing outward from the substrate surface. For such aligned nanotubes, the total contact area of BNNTs with water droplet is small, with air pockets trapped between BNNTs (heterogeneous wetting regime in Figure 1). However, such morphology of BNNTs started to distort toward flattening after annealing at  $T > 500$   $^{\circ}\text{C}$ , probably due to thermal stress relaxation at the bases of BNNTs in contact with the Si substrates. This morphology distortion and removal of the organic adsorbates are responsible for a gradual decrease in contact angle with annealing temperature in Figure 8a. After annealing at  $T > 750$   $^{\circ}\text{C}$ , BNNTs are bundled and flattened and exposed a larger contact area of nanotubes to the water droplet, which helps water to penetrate the network of nanotubes. The effect of high surface energy becomes dominant as now the adsorbates are removed and the contact area on BNNTs has increased. These are the reasons for a sharp decrease of contact angle shown in Figure 8a. Flattening of the BNNTs coatings alone is not the only reason for the changes in contact angle observed here because flattened BNNT samples are still hydrophobic with contact angle  $> 130^{\circ}$ <sup>37</sup> as also shown in Table 2 for samples after wet cleaning. The SEM images of one of the BNNT films used after its annealing at 850  $^{\circ}\text{C}$  provide evidence of bundling of the nanotubes (Figure 8b,c). Finally, the larger statistical variation of contact angles after annealing at  $T > 750$   $^{\circ}\text{C}$  is probably due to the spatial randomness of the flattening process during contact angle measurements.

In short, we found that high-temperature treatment induces hydrophilization of our BNNT samples. To further understand the mechanism, we coated the sample treated at 850  $^{\circ}\text{C}$  with a

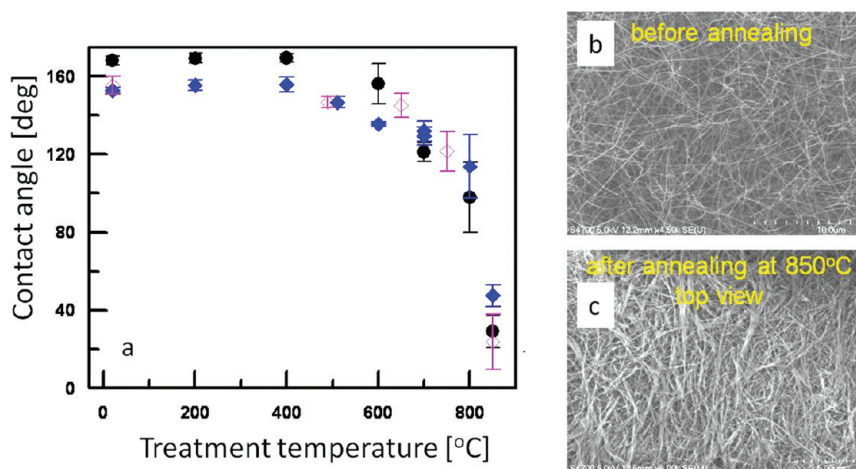


**Figure 8.** (a) The initial contact angles measured 10 min after the heat treatment in argon ambient for samples coated with short (●) and long (◇) BNNTs. Those measured from a sample coated with long BNNTs after heat treatment in air are shown in filled diamonds. Typical SEM images (top view) of samples coated with long BNNTs before (b) and after (c) annealing at 850 °C.

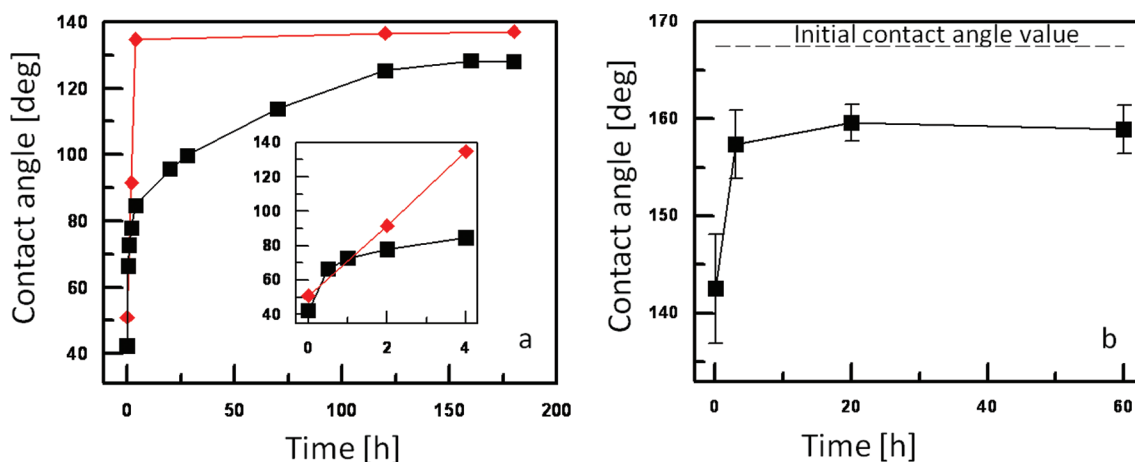


**Figure 9.** (a) Time-dependent evolution of contact angle for sample coated with long BNNTs and exposed to ambient air (◆) and dry nitrogen (■) after heat treatment at 850 °C. Inset shows contact angle versus time dependence in the first 4 h. (b) Restoration of superhydrophobicity of a sample coated with long BNNTs after annealing at 500 °C in Ar. Dashed line marks the initial contact angle value of the same sample before it was annealed.

fluorosilane hydrophobic agent ( $\text{CF}_3(\text{CF}_2)_5\text{CH}_2\text{O}(\text{CH}_2)_3\text{Si}(\text{OCH}_3)_3$ ) by adsorption from the solution as described in ref 44. As expected, adsorption of fluorosilane increased the contact angles from 18° to 30° after heat treatments to 140–145°. This result proved that hydrophobicity of the BNNT sample is due to the presence of alien molecules on BNNTs. Superhydrophobic state with  $\theta > 150^\circ$  could not be restored in these tests due to further bundling of BNNTs during the coating process. We also found that h-BN film coated with the fluorosilane modifier showed contact angles of 105–108°. These results evidently indicate that hydrophobic state can be obtained even for h-BN films if the surface energy is reduced by adsorption of hydrophobic agents.

Let us revisit the IR spectra (Figure 6) collected from samples annealed at 500 and 850 °C. As follows from Figure 6, characteristic peaks of  $\text{CH}_{(n)}$  groups of organic contaminants<sup>55</sup> essentially change after annealing at temperature  $T > 500^\circ\text{C}$ , thus indicating that the initial organic contaminants were removed already at 500 °C. Each of these spectra was collected by more than 800 scans in more than 1 h. As the result, we expect that new hydrocarbon contaminants may be reabsorbed on the heat-treated nanotubes during spectroscopic study and

initiate new IR spectra. To examine this hypothesis, a series of experiments were conducted to understand the evolution of wettability of freshly heat treated samples. Our results in Figure 9 unambiguously indicate that hydrophobization of BNNTs is due to spontaneous adsorption of airborne adsorbates after their heat treatments at 850 °C (Figure 9a) and 500 °C (Figure 9b). As shown in Figure 9a, contact angles for the sample exposed to air increased quickly from ~50° to >135° within 4 h after the heat treatment and remained stable thereafter. The process of hydrophobization is slower when the samples were kept in pure nitrogen atmosphere. However, because the measurement of contact angle was made outside in room ambient, a gradual increase of contact angle with time still took place. These trends were qualitatively reproducible for many samples with some variation in contact angle values. In general, a highly hydrophobic state was restored within a few days of exposition for samples kept in nitrogen ambient. For samples kept in laboratory air, the transition from hydrophilic to hydrophobic state can even occur within 1 h after the heat treatment. The increasing contact angles in air after heat treatment indicate the strong affinity of both short and long

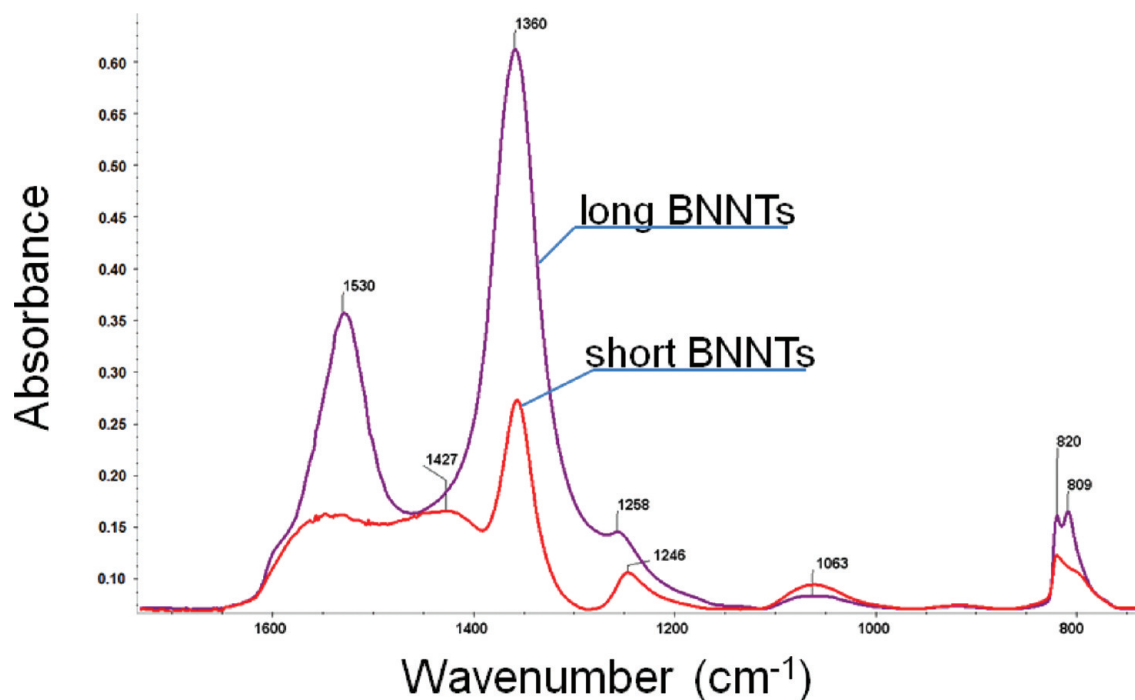


Figure 10. IR absorbance spectra of samples coated with long and short BNNTs.

BNNTs in adsorbing organic contaminants to reduce the surface energy of the nanotubes.

In summary, we showed that high temperature heat treatment could make BNNTs hydrophilic. However, the hydrophobicity of BNNT samples can be restored by spontaneous adsorption of organic adsorbates from the laboratory air. Flat surfaces of thin h-BN films did not exhibit the same affinity to organic adsorbates and thus remained hydrophilic with the highest water contact angles below  $60^\circ$ . Previous reports indeed suggested that adsorption of organic molecules occurs more easily on highly curved surfaces of nanoparticles than on flat surfaces, largely due to effects of increased surface potential.<sup>56–58</sup> However, the differences in adsorption of organics reported in the literature are probably not sufficient to trigger a jump in water contact angle from  $55^\circ$  to over  $90^\circ$ . We expect, therefore, that enhancement of hydrophobic properties of BNNTs as compared to flat surfaces is the result of the combined effect of organic adsorbates and high curvature of the nanotubes.

## CONCLUSIONS

The origins of superhydrophobicity of BNNTs have been identified, that is, the loosely packed nanotubular structures with high surface curvatures, and the hydrocarbon adsorbates. These two origins are correlated. The high surface energy of BN materials is enhanced in BNNTs due to their large surface curvatures. This has increased the affinity of BNNTs to adsorb airborne hydrocarbon molecules, which in turn would reduce the surface energy of BNNTs and make them hydrophobic. We have demonstrated that this superhydrophobic state is thermodynamically stable. Because of the large surface areas offered by the nanotubular structures, freshly prepared or heat treated BNNT coatings could quickly trap the hydrocarbon adsorbates in the atmosphere. The high adsorption affinity of BNNTs to these organic adsorbates provides “a green chemical

route” in maintaining the superhydrophobic state of BNNT coatings in ambient conditions.

On the basis of these findings, it is now possible to explain the discrepancy between the theoretically predicted hydrophilicity of boron nitride materials and the experimentally verified superhydrophobicity of BNNT coatings, where the adsorption of airborne hydrocarbon adsorbates has played an important role.

## APPENDIX

Grazing angle FTIR spectroscopy was used to evaluate our samples in the range of  $700\text{--}1700\text{ cm}^{-1}$ . The typical absorbance spectra of samples coated with long and short BNNTs are shown in Figure 10. Both samples induced absorption bands at  $1360$  and  $1530\text{ cm}^{-1}$  and the doublet at  $809\text{--}820\text{ cm}^{-1}$ , which are associated with in-plane B–N stretching along the tube length, in-plane B–N stretching along the circumference of the nanotubes, and out-of-plane radial buckling of BNNTs, respectively.<sup>38</sup> In addition, we also detected absorption bands not belonging to BNNTs. For example, the band at  $1065\text{ cm}^{-1}$  may be associated with the TO mode of  $\text{sp}^3$  BN bonds.<sup>59</sup> The band with maximum of absorbance around  $1250\text{ cm}^{-1}$  may be interpreted as C–N or B–C bonds due to minute carbon contamination.<sup>60</sup> The bands revealed in the spectra of short BNNTs centered at about  $1427$  and  $921\text{ cm}^{-1}$  can be assigned to B–O stretching vibrations in B–O–N and B–O–Si groups.<sup>61</sup> The oxygen traces were also detected on the EDX spectra (not shown here). The presence of B–O groups, characterized by strong hydration affinity, was also detected in the experiments with long-term exposure of coating in saturated vapor pressure as discussed in the main text.

## ■ AUTHOR INFORMATION

## Corresponding Author

\*Fax: (+7 495) 952 5308. E-mail: boinovich@mail.ru (L.B.B.), ykyap@mtu.edu (Y.K.Y.).

## ■ ACKNOWLEDGMENTS

L.B.B., A.M.E., and A.S.P. acknowledge the support from the Presidential program of support for the Leading Scientific Schools (Project NSh-7853.2010.3), and from the Program P-22 of Russian Academy of Sciences. Y.K.Y. is grateful for the support from the National Science Foundation (CAREER Award No. 0447555) and the Department of Energy, the Office of Basic Energy Sciences (Grant No. DEFG02-06ER46294).

## ■ REFERENCES

- (1) Barthlott, W.; Neinhuis, C. Purity of the sacred lotus, or escape from contamination in biological surfaces. *Planta* **1997**, *202*, 1–8.
- (2) Neinhuis, C.; Barthlott, W. Characterization and distribution of water-repellent, self-cleaning plant surfaces. *Ann. Bot.* **1997**, *79*, 667–677.
- (3) Wagner, T.; Neinhuis, C.; Barthlott, W. Wettability and contaminability of insect wings as a function of their surface sculptures. *Acta Zool.* **1996**, *77*, 213–225.
- (4) Hu, H. M. S.; Watson, G. S.; Cribb, B. W.; Watson, J. A. Non-wetting wings and legs of the crane fly aided by fine structures of the cuticle. *J. Exp. Biol.* **2011**, *214*, 915–920.
- (5) Watson, G. S.; Cribb, B. W.; Watson, J. A. How micro/nanoarchitecture facilitates anti-wetting: an elegant hierarchical design on the termite wing. *ACS Nano* **2010**, *4*, 129–136.
- (6) Liu, Y. Y.; Chen, X. Q.; Xin, J. H. Hydrophobic duck feathers and their simulation on textile substrates for water repellent treatment. *Bioinspiration Biomimetics* **2008**, *3*, 4.
- (7) Bormashenko, E.; Bormashenko, Y.; Stein, T.; Whyman, G. Why do pigeon feathers repel water? Hydrophobicity of penna, Cassie-Baxter wetting hypothesis and Cassie-Wenzel capillarity-induced wetting transition. *J. Colloid Interface Sci.* **2007**, *311*, 212–216.
- (8) Balmert, A.; Bohn, H. F.; Ditsche-Kuru, P.; Barthlott, W. Dry under water: comparative morphology and functional aspects of air-retaining insect surfaces. *J. Morphol.* **2011**, *272*, 442–451.
- (9) Barthlott, W.; Schimmel, T.; Wiersch, S.; Koch, K.; Brede, M.; Barczewski, M.; Walheim, S.; Weis, A.; Kaltenmaier, A.; Leder, A.; Bohn, H. F. The Salvinia paradox: superhydrophobic surfaces with hydrophilic pins for air retention under water. *Adv. Mater.* **2010**, *22*, 2325–2328.
- (10) Zheng, Q. S.; Yu, Y.; Feng, X. Q. The role of adaptive deformation of water strider leg in its walking on water. *J. Adhes. Sci. Technol.* **2009**, *23*, 493–501.
- (11) Watson, G. S.; Cribb, B. W.; Watson, J. A. Experimental determination of the efficiency of nanostructuring on non-wetting legs of the water strider. *Acta Biomater.* **2010**, *6*, 4060–4064.
- (12) Feng, X. Q.; Gao, X. F.; Wu, Z. N.; Jiang, L.; Zheng, Q. S. Superior water repellency of water strider legs with hierarchical structures: Experiments and analysis. *Langmuir* **2007**, *23*, 4892–4896.
- (13) Quere, D. Non-sticking drops. *Rep. Prog. Phys.* **2005**, *68*, 2495–2532.
- (14) Callies, M.; Quere, D. On water repellency. *Soft Matter* **2005**, *1*, 55–61.
- (15) Marmur, A. From hydrophilic to superhydrophobic: Theoretical conditions for making high-contact-angle surfaces from low-contact-angle materials. *Langmuir* **2008**, *24*, 7573–7579.
- (16) Chhatre, S. S.; Tuteja, A.; Choi, W.; Revaux, A.; Smith, D.; Mabry, J. M.; McKinley, G. H.; Cohen, R. E. Thermal annealing treatment to achieve switchable and reversible oleophobicity on fabrics. *Langmuir* **2009**, *25*, 13625–13632.
- (17) Cui, X. S.; Li, W. On the possibility of superhydrophobic behavior for hydrophilic materials. *J. Colloid Interface Sci.* **2010**, *347*, 156–162.
- (18) Fadeeva, E.; Truong, V. K.; Stiesch, M.; Chichkov, B. N.; Crawford, R. J.; Wang, J.; Ivanova, E. P. Bacterial retention on superhydrophobic titanium surfaces fabricated by femtosecond laser ablation. *Langmuir* **2011**, *27*, 3012–3019.
- (19) Karlsson, M.; Forsberg, P.; Nikolajeff, F. From hydrophilic to superhydrophobic: fabrication of micrometer-sized nail-head-shaped pillars in diamond. *Langmuir* **2010**, *26*, 889–893.
- (20) Watanabe, T. Wettability of ceramic surfaces – A wide range control of surface wettability from super hydrophilicity to super hydrophobicity, from static wettability to dynamic wettability. *J. Ceram. Soc. Jpn.* **2009**, *117*, 1285–1292.
- (21) Marmur, A. Wetting on hydrophobic rough surfaces: To be heterogeneous or not to be? *Langmuir* **2003**, *19*, 8343–8348.
- (22) Wenzel, R. Resistance of solid surfaces to wetting by water. *Ind. Eng. Chem.* **1936**, *28*, 988–994.
- (23) Derjaguin, B. V. On the dependence of the contact angle on the microrelief or roughness of a wetted solid surface. *C. R. (Dokl.) Acad. Sci. URSS* **1946**, *51*, 361–364.
- (24) Cassie, A. B.; Baxter, S. Wettability of porous surfaces. *Trans. Faraday Soc.* **1944**, *40*, 546–551.
- (25) Marmur, A. The lotus effect: superhydrophobicity and metastability. *Langmuir* **2004**, *20*, 3517–3519.
- (26) Patankar, N. A. On the modeling of hydrophobic contact angles on rough surfaces. *Langmuir* **2003**, *19*, 1249–1253.
- (27) He, B.; Patankar, N. A.; Lee, J. Multiple equilibrium droplet shapes and design criterion for rough hydrophobic surfaces. *Langmuir* **2003**, *19*, 4999–5003.
- (28) Neumann, A. W.; Good, R. J. Thermodynamics of contact angles. 1. Heterogeneous solid surfaces. *J. Colloid Interface Sci.* **1972**, *38*, 341–358.
- (29) Schwartz, L. W.; Garoff, S. Contact-angle hysteresis and the shape of the 3-phase line. *J. Colloid Interface Sci.* **1985**, *106*, 422–437.
- (30) Fang, C. P.; Drelich, J. Theoretical contact angles on a nano-heterogeneous surface composed of parallel apolar and polar strips. *Langmuir* **2004**, *20*, 6679–6684.
- (31) Tuteja, A.; Choi, W.; Mabry, J. M.; McKinley, G. H.; Cohen, R. E. Robust omniphobic surfaces. *Proc. Natl. Acad. Sci. U.S.A.* **2008**, *105*, 18200–18205.
- (32) Choi, W.; Tuteja, A.; Chhatre, S.; Mabry, J. M.; Cohen, R. E.; McKinley, G. H. Fabrics with tunable oleophobicity. *Adv. Mater.* **2009**, *21*, 2190.
- (33) Bormashenko, E.; Pogreb, R.; Whyman, G.; Erlich, M. Cassie-wenzel wetting transition in vibrating drops deposited on rough surfaces: Is the dynamic cassie-wenzel wetting transition a 2D or 1D affair? *Langmuir* **2007**, *23*, 6501–6503.
- (34) Daniel, S.; Sircar, S.; Gliem, J.; Chaudhury, M. K. Ratcheting motion of liquid drops on gradient surfaces. *Langmuir* **2004**, *20*, 4085–4092.
- (35) Quere, D.; Lafuma, A.; Bico, J. Slippery and sticky microtextured solids. *Nanotechnology* **2003**, *14*, 1109–1112.
- (36) Li, L. H.; Chen, Y. Superhydrophobic properties of nonaligned boron nitride nanotube films. *Langmuir* **2010**, *26*, 5135–5140.
- (37) Lee, C. H.; Drelich, J.; Yap, Y. K. Superhydrophobicity of boron nitride nanotubes grown on silicon substrates. *Langmuir* **2009**, *25*, 4853–4860.
- (38) Lee, C. H.; Wang, J. S.; Kayatsha, V. K.; Huang, J. Y.; Yap, Y. K. Effective growth of boron nitride nanotubes by thermal chemical vapor deposition. *Nanotechnology* **2008**, *19*, 455605.
- (39) Ooi, N.; Adams, J. B. Ab initio studies of the cubic boron nitride (110) surface. *Surf. Sci.* **2005**, *574*, 269–286.
- (40) Ruuska, H.; Larsson, K. Surface reactivities of (111), (100), and (110) planes of c-BN: A quantum mechanical approach. *Diamond Relat. Mater.* **2007**, *16*, 118–123.
- (41) Lee, C. H.; Xie, M.; Kayastha, V.; Wang, J. S.; Yap, Y. K. Patterned growth of boron nitride nanotubes by catalytic chemical vapor deposition. *Chem. Mater.* **2010**, *22*, 1782–1787.
- (42) Emelyanenko, A. M.; Boinovich, L. B. Application of dynamic thresholding of video images for measuring the interfacial tension of liquids and contact angles. *Instrum. Exp. Tech.* **2002**, *45*, 44–49.

(43) Emel'yanenko, A. M.; Boinovich, L. B. The use of digital processing of video images for determining parameters of sessile and pendant droplets. *Colloid J.* **2001**, *63*, 159–172.

(44) Boinovich, L.; Emelyanenko, A. M.; Pashinin, A. S. Analysis of long-term durability of superhydrophobic properties under continuous contact with water. *ACS Appl. Mater. Interfaces* **2010**, *2*, 1754–1758.

(45) Wu, S. *Polymer Interface and Adhesion*; Marcel Dekker, Inc.: New York and Basel, 1982.

(46) Adamson, A. W. *Physical Chemistry of Surfaces*, 5th ed.; John Wiley & Sons, Inc.: New York, 1990.

(47) Spiesser, A.; Chong, Y. M.; Leung, K. M.; Abel, G.; Ross, G. G.; Walzak, M. J.; Jacklin, R.; Lau, W. M.; Zhang, W. J.; Bello, I. Surface free energy of cubic boron nitride films deposited on nanodiamond. *J. Phys. Chem. C* **2007**, *111*, 12768–12772.

(48) Keunecke, M.; Yamamoto, K.; Bewilogua, K. Mechanical and tribological properties of cBN films on silicon and tungsten carbide substrates. *Thin Solid Films* **2001**, *398*, 142–149.

(49) Yum, K.; Yu, M. F. Measurement of wetting properties of individual boron nitride nanotubes with the Wilhelmy method using a nanotube-based force sensor. *Nano Lett.* **2006**, *6*, 329–333.

(50) Boinovich, L.; Emelyanenko, A. Wetting and surface forces. *Adv. Colloid Interface Sci.* **2011**, *165*, 60–69.

(51) Della Volpe, C.; Maniglio, D.; Morra, M.; Siboni, S. The determination of a “stable-equilibrium” contact angle on heterogeneous and rough surfaces. *Colloids Surf., A* **2002**, *206*, 47–67.

(52) Boinovich, L.; Emelyanenko, A. M. The prediction of wettability of curved surfaces on the basis of the isotherms of the disjoining pressure. *Colloids Surf., A* **2011**, *383*, 10–16.

(53) Thundat, T.; Zheng, X. Y.; Chen, G. Y.; Sharp, S. L.; Warmack, R. J.; Schowalter, L. J. Characterization of atomic-force microscope tips by adhesion force measurements. *Appl. Phys. Lett.* **1993**, *63*, 2150–2152.

(54) Zhi, C. Y.; Bando, Y.; Tang, C. C.; Xie, R. G.; Sekiguchi, T.; Golberg, D. Perfectly dissolved boron nitride nanotubes due to polymer wrapping. *J. Am. Chem. Soc.* **2005**, *127*, 15996–15997.

(55) Smith, A. L. *Applied Infrared Spectroscopy: Fundamentals, Techniques, and Analytical Problem-Solving*; Wiley: New York, 1979.

(56) Zhang, H. Z.; Penn, R. L.; Hamers, R. J.; Banfield, J. F. Enhanced adsorption of molecules on surfaces of nanocrystalline particles. *J. Phys. Chem. B* **1999**, *103*, 4656–4662.

(57) Grassian, V. H. When size really matters: size-dependent properties and surface chemistry of metal and metal oxide nanoparticles in gas and liquid phase environments. *J. Phys. Chem. C* **2008**, *112*, 18303–18313.

(58) Pettibone, J. M.; Cwiertny, D. M.; Scherer, M.; Grassian, V. H. Adsorption of organic acids on TiO<sub>2</sub> nanoparticles: Effects of pH, nanoparticle size, and nanoparticle aggregation. *Langmuir* **2008**, *24*, 6659–6667.

(59) Yap, Y. K.; Aoyama, T.; Kida, S.; Mori, Y.; Sasaki, T. Synthesis of adhesive c-BN films in pure nitrogen radio-frequency plasma. *Diamond Relat. Mater.* **1999**, *8*, 382–385.

(60) Yap, Y. K.; Yoshimura, M.; Mori, Y.; Sasaki, T. Hybridized boron-carbon nitride fibrous nanostructures on Ni substrates. *Appl. Phys. Lett.* **2002**, *80*, 2559–2561.

(61) Yasui, H.; Awazu, K.; Ikenaga, N.; Sakudo, N. Synthesis and characterization of BN thin films prepared by plasma MOCVD with organoboron precursors. *Vacuum* **2008**, *83*, 582–584.